SUPPLEMENTARY MATERIALS AND METHODS

Measuring depigmentation

The mean luminosity for the ventral area of mice was measured in Adobe Photoshop CC 2017 (Adobe, San Jose, CA) with a fully pigmented pelage representing 0% depigmentation and a fully depigmented pelage representing 100% depigmentation. The depigmentation was graphed over time, and the slopes were calculated and compared between the antibiotic and control groups.

Immunostaining

For CD3e, Biotin Block (ScyTek Laboratories) was added after SuperBlock, and sections were incubated with bio-tinylated antibody 145-2C11 to mouse CD3ε (Becton Dickinson Biosciences, Franklin Lakes, NJ). For CD4 and CD8a staining, ileum sections were incubated with RM4-5 to mouse CD4 (BD Biosciences, San Jose, CA) or 53−6.7 to mouse CD8a (BD Biosciences). For TRP-2 staining, skin sections were incubated with antibody D-18 to TRP-2 (Santa Cruz Biotechnology, Santa Cruz, CA). CD3ε was detected with horseradish peroxidase (HRP)-labeled strep-tavidin (SouthernBiotech, Birmingham, AL). CD4 and CD8a were detected with HRP-labeled goat anti-rat sec-ondary antibody (SouthernBiotech) for ileum sections, and TRP-2 was detected with HRP-labeled swine anti-goat secondary antibody (SouthernBiotech). CD3ε, CD4, CD8a, and TRP-2 were detected with HRP-labeled strep-tavidin (SouthernBiotech), developed with amino-ethylcarbazole substrate (Abcam, Cambridge, United Kingdom), and counterstained with Harris hematoxylin (Sigma-Aldrich) where necessary. For CD4 and CD8a staining of the skin, the sections were incubated with Alexa Fluor 488)-labeled GK1.5 to mouse CD4 (BioLegend) or biotinylated 53-6.7 to mouse CD8a (BioLegend), which was detected with phycoerythrin (PE)-labeled streptavidin (SouthernBiotech) with nuclear detection via DAPI (BD Biosciences) staining. For FoxP3 staining Alexa Fluor 488-labeled MF-14 to mouse FoxP3 (BioLegend) and PE-labeled anti-CD3ε (BioLegend) were utilized, followed by 4′,6-diamidino-2-phenylindole (DAPI) (BD Biosciences) nuclear staining. For TUNEL staining, the sections were fixed in 1% paraformaldehyde in phosphate buffered saline (Electron Microscopy Sciences, Hatfield, PA) and per-meabilized in 2:1 ethanol:acetic acid before incubation with TdT enzyme and anti-digoxigenin conjugate. The development of TUNEL staining was performed via ami-noethylcarbazole substrate (Abcam) and sections were counter stained with Mayer's hematoxylin (Thermo Fisher Scientific) and blued in Scott's tap water (Sigma-Aldrich).

Immunoblotting

The membranes were immunostained with the following antibodies: anti- inducible heat shock protein 70 [C92F3A-5] (Enzo Life Sciences, Farmingdale, NY), anti-4 Hydrox-ynonenal (4-HNE) (Abcam), and anti-actin [C4/actin] (BD Biosciences). Secondary antibodies included HRP-labeled anti-mouse IgG1 (Southern Biotech) for the recognition of inducible heat shock protein 70 and actin and anti-rabbit IgG (Dako [Agilent Technologies], Santa Clara, CA) for 4-HNE, and all were developed with an enhanced chem-iluminescence substrate (Thermo Fisher Scientific) and film (Denville Scientific [Thomas Scientific], Swedesboro, NJ). The analysis was performed via ImageJ on scanned (Epson, Suwa, Japan) images of the film, and the relative levels compared to actin were calculated.

Flow cytometry

Surface staining included anti-CD45 BB515 (30-F11), CD3 BUV395 (145-2C11), CD4 BUV737 (GK1.5; all BD Biosciences), CD8 BV786 (53-6.7; Biolegend) antibodies. The cells were fixed and permeabilized with BD Cytofix/Cytoperm kit (BD Biosciences) per the manufacturer's instructions before intracellular cytokine staining with anti-IFN-γ APC (XMG1.2) and anti-IL-17A PE (TC11-18H10.1; both Biolegend) antibodies.

16S rRNA amplicon sequencing (sub-operational taxonomic unit)

Forward and reverse reads were merged using PEAR (Zhang et al., 2014). Ambiguous nucleotides were removed from the ends and reads, and internal ambiguous nucleotides were discarded. The primer sequences were identified using a Smith-Watermann alignment and removed from the sequence. Reads that lacked either primer sequence were discarded. The sequences were then trimmed based on quality scores using a modified Mott algorithm with Phred quality threshold of $P = 0.01$. After trimming. any sequences less than 225 base pairs were discarded. Chimeric sequences were identified and removed using the USEARCH algorithm with a comparison to the Silva v132 reference sequence database.(Edgar, 2010; Glöckner et al., 2017).

The standard QIIME pipline was modified to generate taxonomic summaries using sub-operational taxonomic unit resolution of the sequence dataset (Caporaso et al., 2010; Tikhonov et al., 2015). Briefly, the resulting sequence files were then merged with the sample information. All the sequences were then dereplicated to produce a list of unique sequences. All the sequences that had an abundance of at least 10 counts were designated seed sequences. USEARCH was then used to find the nearest seed sequence for any non-seed sequence with a minimum identity threshold of 98%. For any non-seed sequence that matched a seed sequence, its counts were merged with the seed sequence counts. Any non-seed sequence that did not match a seed sequence would remain an independent sequence.

Taxonomic annotations for the seed and unmatched non-seed sequences were assigned using the USEARCH and Silva v132 reference with a minimum similarity threshold of 90% (Edgar, 2010; Glöckner et al., 2017). To improve the depth of annotation, the standard QIIME assignment algorithm was modified to only consider hits at each taxonomic level that had an assigned name. For example, a reference annotated as "D_0__Bacteria; D_1__Firmicutes; D_2__Clostridia; D_3__Clostridiales; D_4__Ruminococcaceae; D_5__; D_6__" would be considered in the assignment of the taxonomic kingdom through the family but would not be used for the assignment of the genus or species. Furthermore, any hits in the reference database must have had a minimum identity of 97% or 99% to be considered for genus or species level assignment, respectively. Taxonomic

annotations and sequence abundance data were then merged into a single sequence table.

Data at the genus and species level for each sample are presented as a percentage of the total microbiome reads for that sample. Within the gut and skin cohorts, a cut-off was established for each sample, whereby if the genus or species did not represent at least 2% of the total microbiome in any of the samples in that tissue category, it was collapsed into the "other" category. Where species or genera were not able to be sequenced at the taxanomic level of interest, they were considered part of the "other" category for analysis purposes.

SUPPLEMENTARY REFERENCES

Caporaso JG, Kuczynski J, Stombaugh J, Bittinger K, Bushman FD, Costello EK, et al. QIIME allows analysis of high-throughput community sequencing data. Nat Methods 2010;7:335–6.

Edgar RC. Search and clustering orders of magnitude faster than BLAST. Bioinformatics 2010;26:2460–1.

Glöckner FO, Yilmaz P, Quast C, Gerken J, Beccati A, Ciuprina A, et al. 25 years of serving the community with ribosomal RNA gene reference databases and tools. J Biotechnol 2017;261:169–76.

Tikhonov M, Leach RW, Wingreen NS. Interpreting 16S metagenomic data without clustering to achieve sub-OTU resolution. ISME J 2015;9:68–80.

Zhang J, Kobert K, Flouri T, Stamatakis A. PEAR: a fast and accurate Illumina Paired-End reAd mergeR. Bioinformatics 2014;30:614–20.

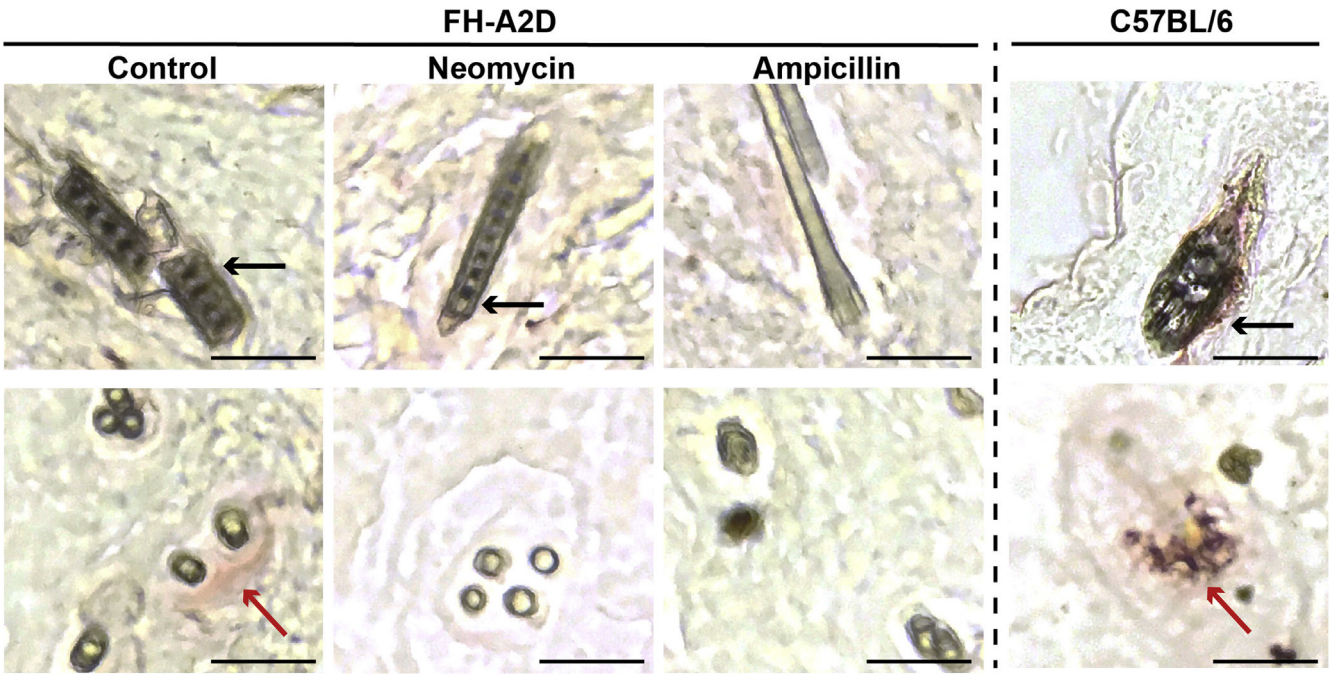

Supplementary Figure S1. Depigmentation is accompanied by melanocyte loss in antibiotic-treated FH-A2D mice. Skin from control and neomycin treated but not ampicillin-treated FH-A2D mice scanned for 30 weeks showed residual pigmented hair. Only the control FH-A2D mice showed minimal tyrosinase-related protein-2 (TRP-2) staining in the hair follicles, demonstrating lingering melanocytes. C57BL/6 mouse skin is shown for comparison; readily apparent staining for TRP-2 and hair pigmentation is visible. Arrows: TRP-2 staining (red), melanin (black). Bar = 50 μm.

Supplementary Figure S2. Depigmentation is not accompanied by increased oxidative stress. Quantification of (**a**) 4-hydroxy-2-nonenal (4-HNE), a metabolic marker of reactive oxygen species, and (**b**) inducible heat shock protein 70 (HSP70i) expression in colon homogenates. Expression evaluated ± standard deviation in protein isolates from the control, neomycin-, and ampicillin-treated animals. The differences were not significant. Black lines between the different treatment groups demonstrate the rearrangement of lanes from the same membrane to allow for consistent ordering between (**a**) and (**b**). 4-HNE, 4-hydroxy-2-nonenal.

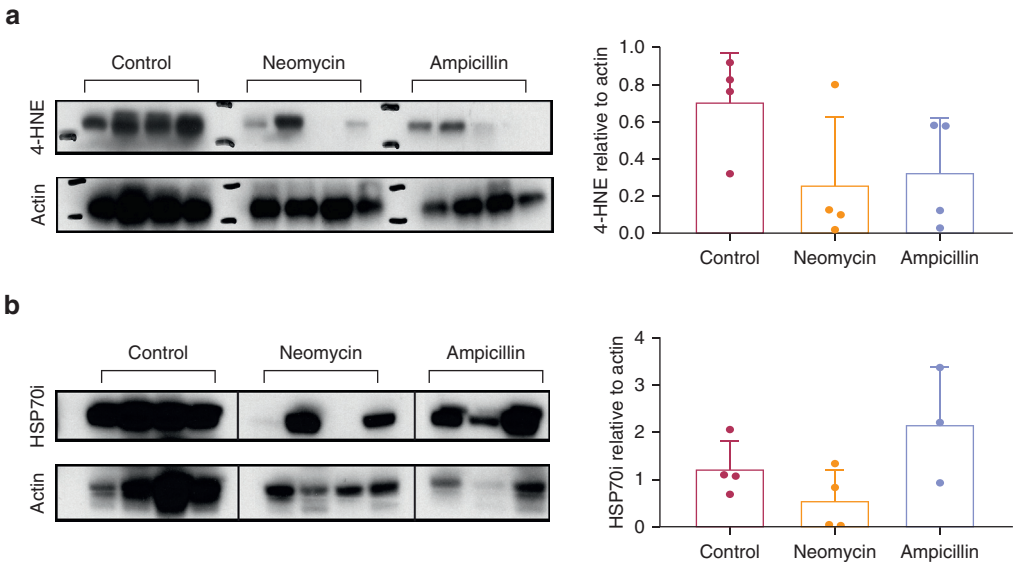

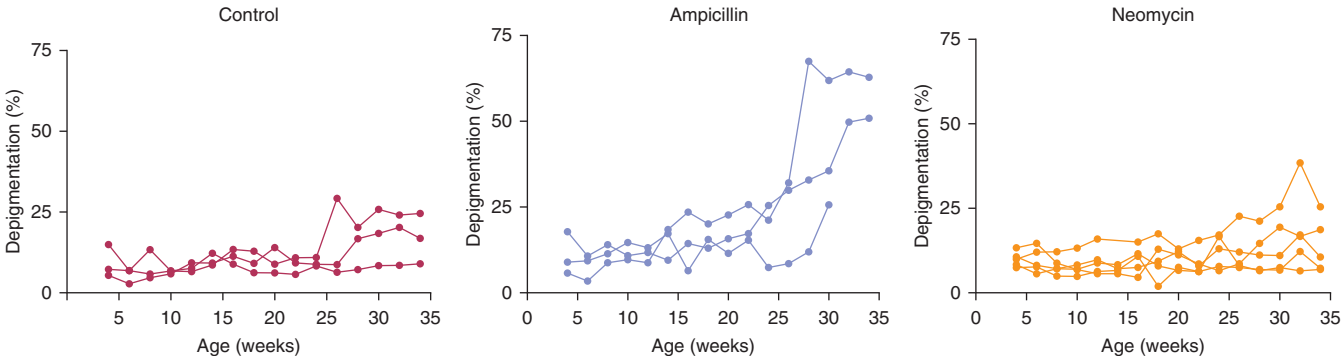

Supplementary Figure S3. Representative samples used to align depigmentation status and the microbiome. Shown are the depigmentation curves for mice providing skin samples to successfully analyze the skin microbiome at the end point by a 16S rRNA analysis.

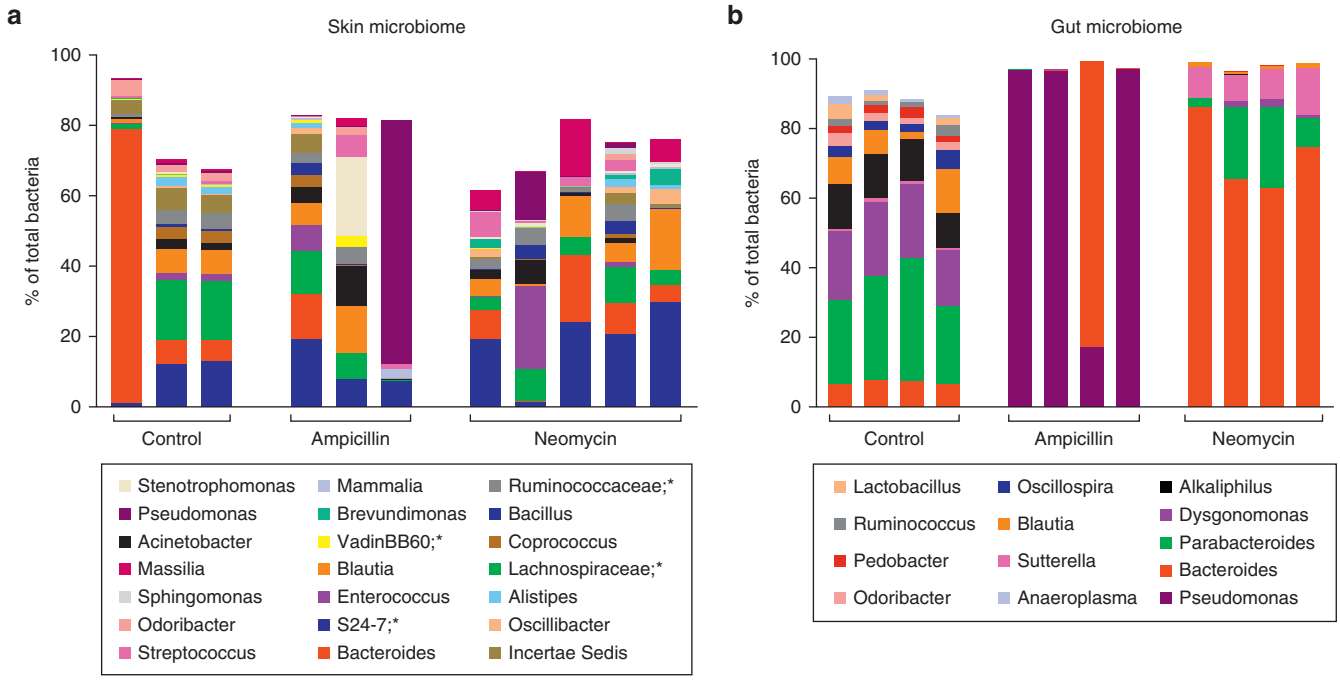

Supplementary Figure S4. Variability among the skin samples is greater than that among the gut samples. The abundance of individual bacterial genera is represented for (**a**) skin samples from control, ampicillin-treated, or neomycin-treated mice at the end point or (**b**) for fecal samples analyzed from mice under long-term antibiotic treatment. *Genus not identifiable.

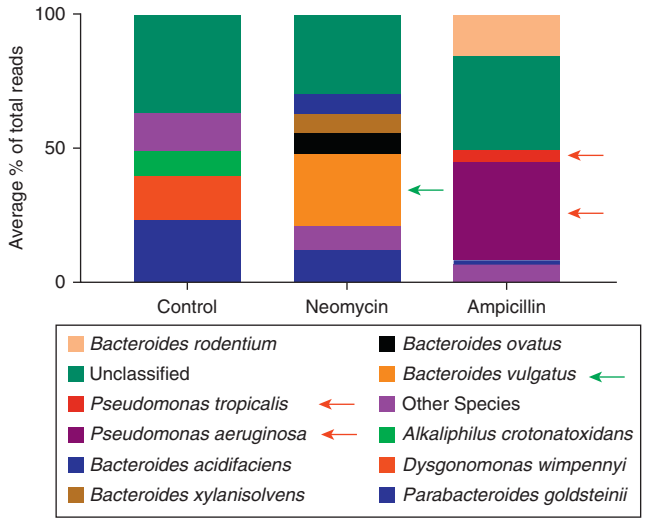

Supplementary Figure S5. *Pseudomonas aeruginosa* and *Pseudomonas tropicalis* correlate with accelerated depignmentation, and *Bacteroides vulgatus* correlates with delayed depigmentation. Overrepresentation of opportunistic *Pseudomonas aeruginosa* and *Pseudomonas tropicalis* species was observed in the feces after ampicillin treatment (red arrows). In contrast, *Bacteroides vulgatus* was abundant in the neomycin-treated animals (green arrow).

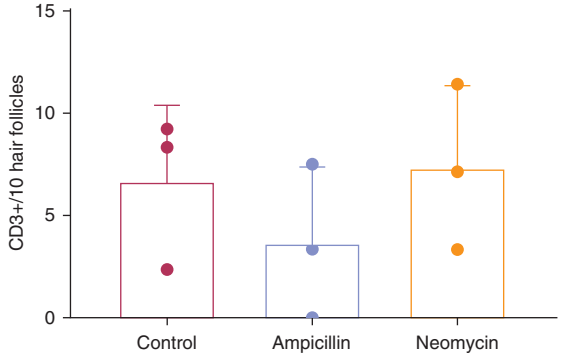

Supplementary Figure S6. T cell abundance is similar among control and antibiotic-treated mice. CD3e (pan T cells) quantified in 10 hair follicles of control or antibiotic-treated mice, showing similar trends as the frequencies per total area of skin.

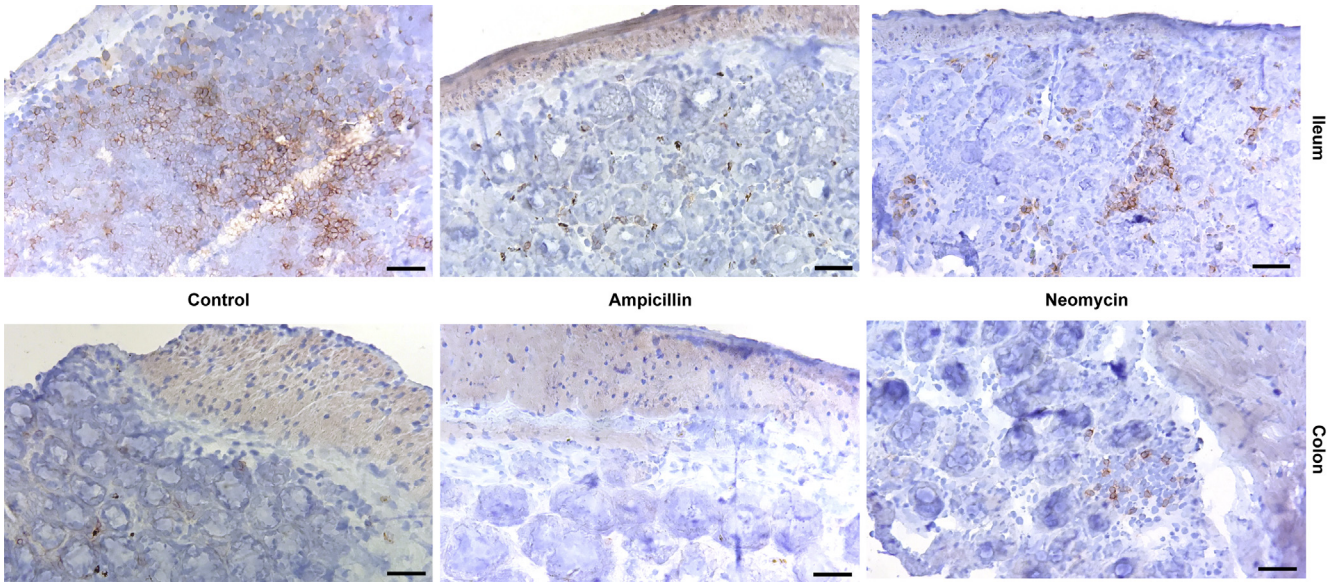

Supplementary Figure S7. Readily apparent differences in the T cell abundance in the ileum after antibiotic treatments. When CD3e pan T cell abundance was compared in the ileum and colon of mice treated with antibiotics versus those with no antibiotics in the drinking water, differences among the treatment groups are readily apparent in the ileum but not the colon. Bar = 50 μm.

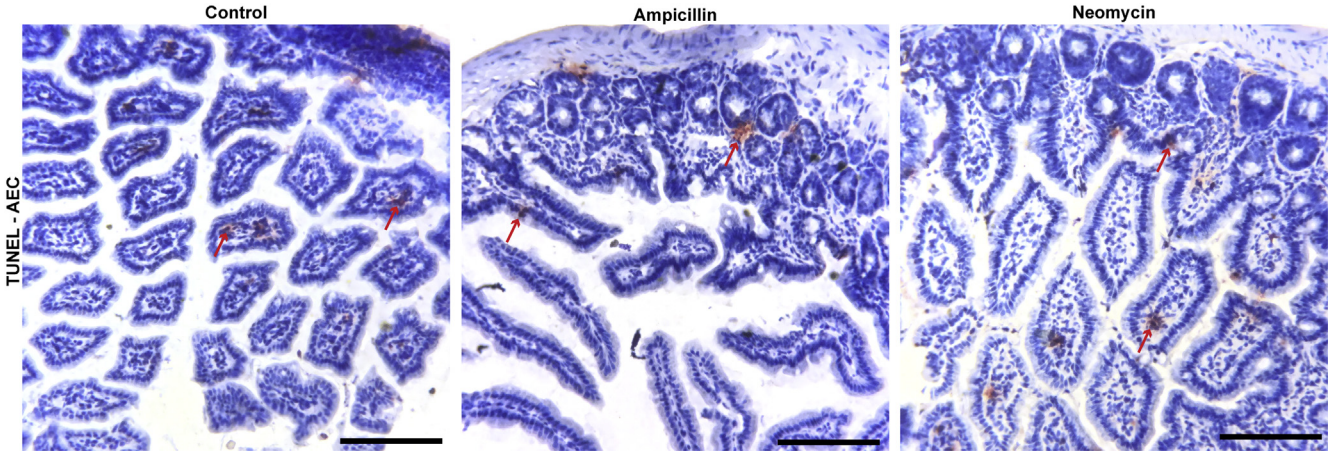

Supplementary Figure S8. TUNEL staining reveals similar rates of apoptosis among treatment groups in the ileum. Apoptosis is shown in tissues from the antibiotic-treated or control mice. Similar levels of apoptosis are found in each treatment group (arrows: examples) when the staining (red) is compared against the hematoxylin+ nuclei (blue), although the location of the dying cells differs. TUNEL staining is found within the villi in the control mice, but the antibiotic-treated mice reveal apoptosis in both the villi and the intervillous space. Bar = 50 μm.

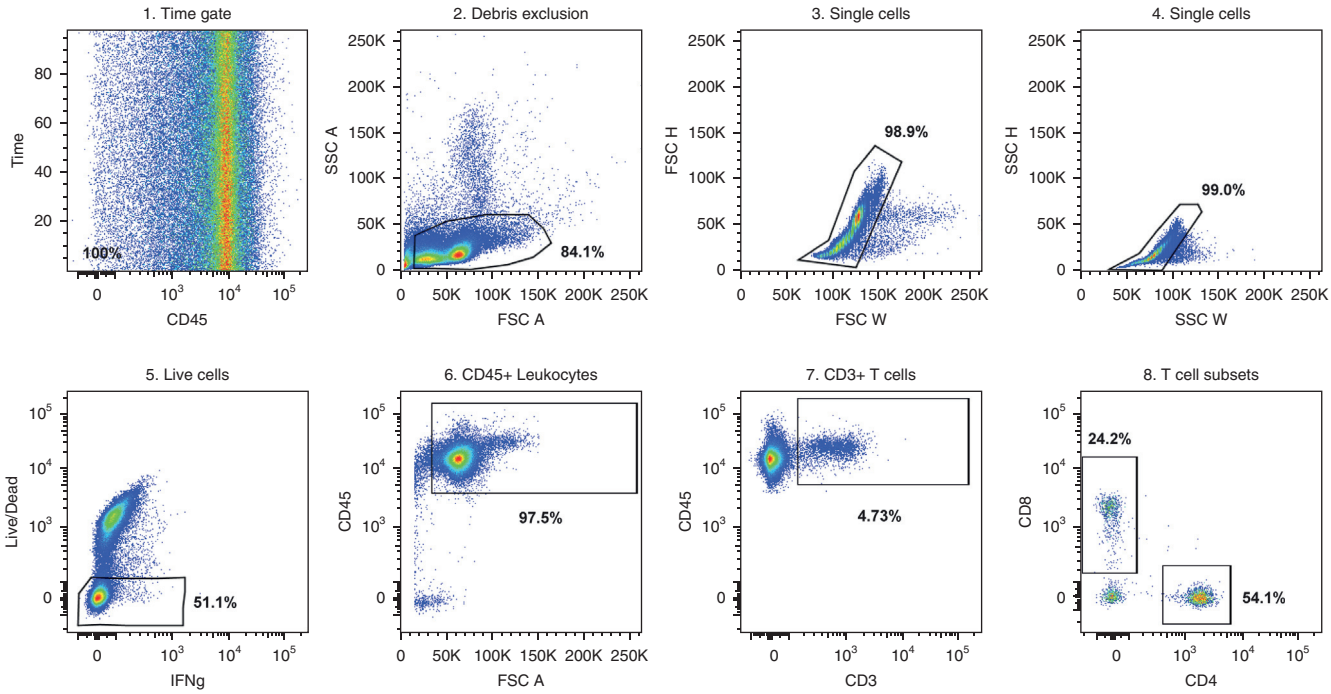

Supplementary Figure S9. CD4+ and CD8+ T cell subsets were identified using a sequential gating strategy. Briefly, a time gate was used to check for flow-rate abnormalities, followed by debris exclusion, two rounds of doublet cell exclusion, and dead cell exclusion. Leukocytes were identified based on the CD45 expression, T cells by the CD3 expression, and finally CD4 and CD8 expression was used to separate the T cell subsets for downstream functional analysis. FSC A, forward scatter area; FSC W, forward scatter width; SSC W, side scatter width.